Structural Elucidation of polydopamine facilitated by ionic liquid solvation

Abhishek Singh[1,2], Thomas G. Mason[1], Zhenzhen Lu[1], Anita J. Hill[3], Steven J. Pas[4], Boon Mia Teo[1], Benny D. Freeman[4] and Ekaterina I. Izgorodina[1,*]

[1]School of Chemistry, Monash University, Clayton, Melbourne, VIC 3800, Australia

[2]IITB-Monash Research Academy, Bombay 400076, India

[3]Manufacturing, CSIRO, Clayton, VIC 3168, Australia

[4] Maritime Division, Defence Science and Technology Group, Department of Defence, 506 Lorimer St Fisherman's Bend, VIC 3207, Australia

[5]Department of Chemical Engineering, The University of Texas at Austin, Austin, TX 78712, USA

† These authors contributed equally to this work

*Corresponding author. katya.pas@monash.edu

This PDF file includes

1. Supplementary Figures S1 to S24
2. Supplementary Tables S1 to S10
3. References

1. Supplementary Figures

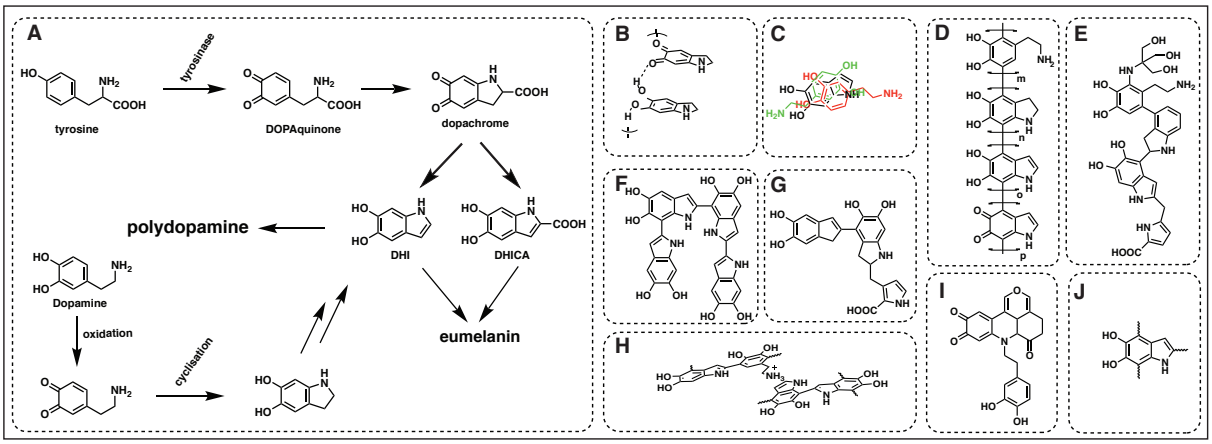

Supplementary Figure 1. (A) Schematic view of eumelanin and pDA-melanin synthetic pathways. Structural models of pDA – B[1], C[2], D[3], E[4], F[5], G[6], H[7], I[8] and J[9] – postulated between 2012 and 2018.

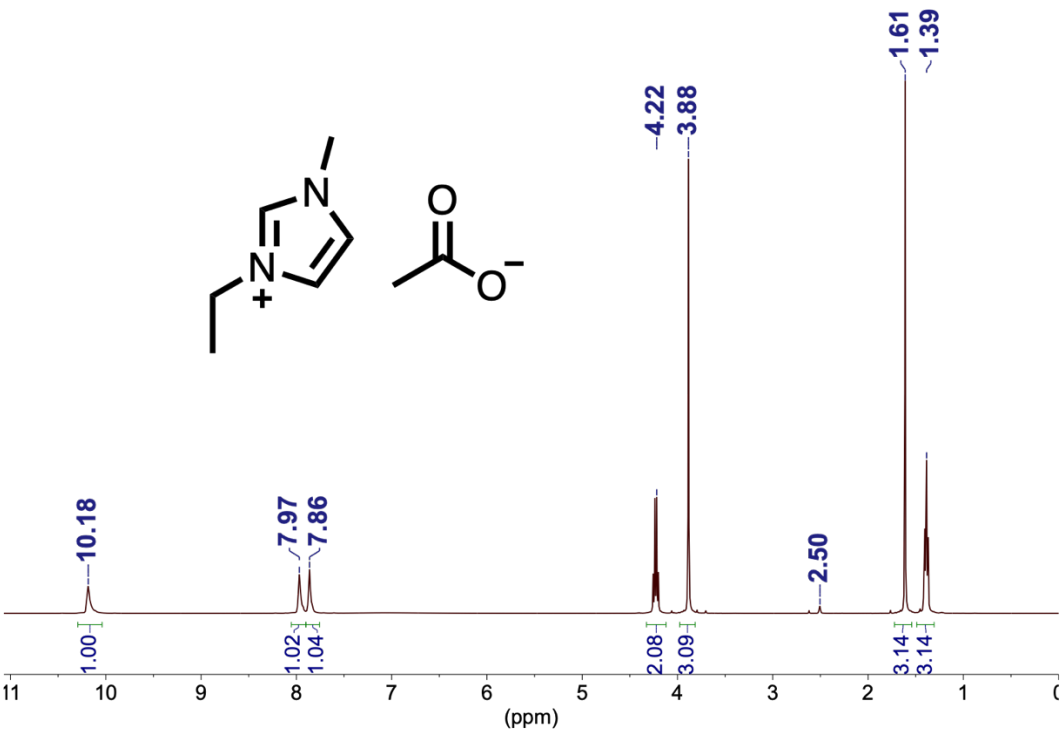

Supplementary Figure 2. ^{1}H-NMR spectra of neat [C_2mim][OAc] and dopamine monomer in DMSO-d_6.

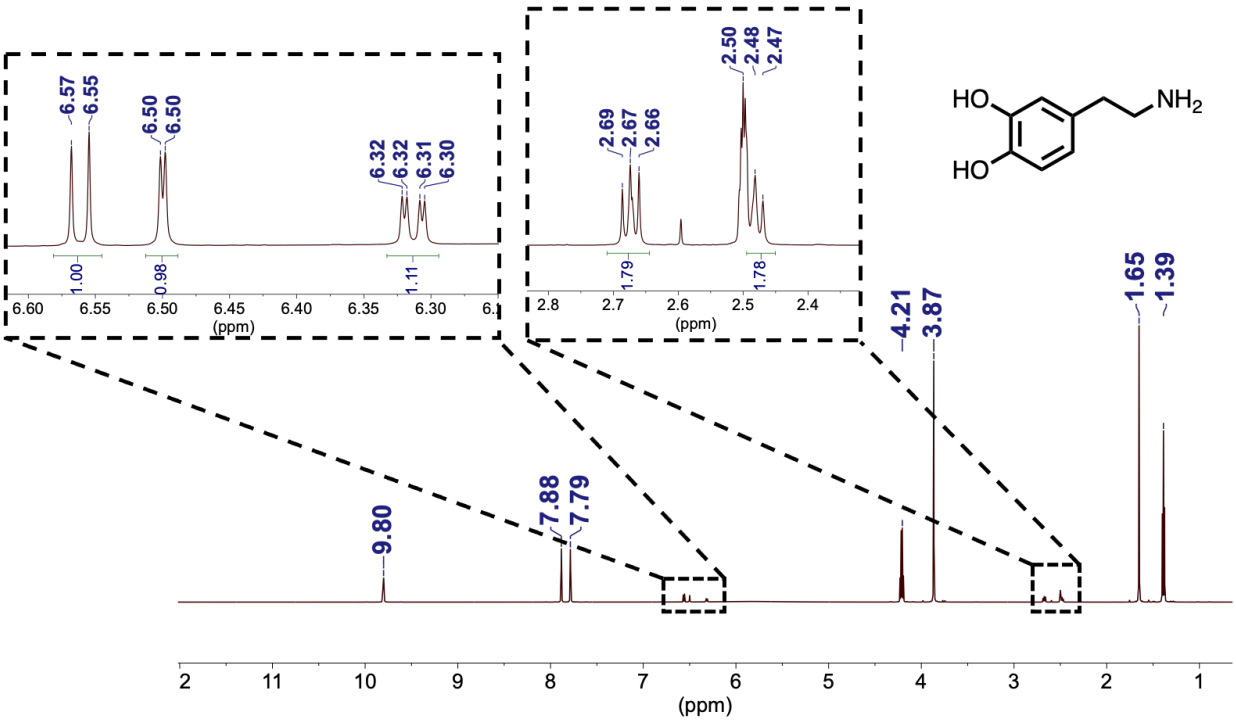

Supplementary Figure 3. ^{1}H-NMR spectra of dopamine hydrochloride dissolved in [C_2mim][OAc] and recorded in DMSO-d_6 (only dopamine signals are shown and zoomed out in the inset.

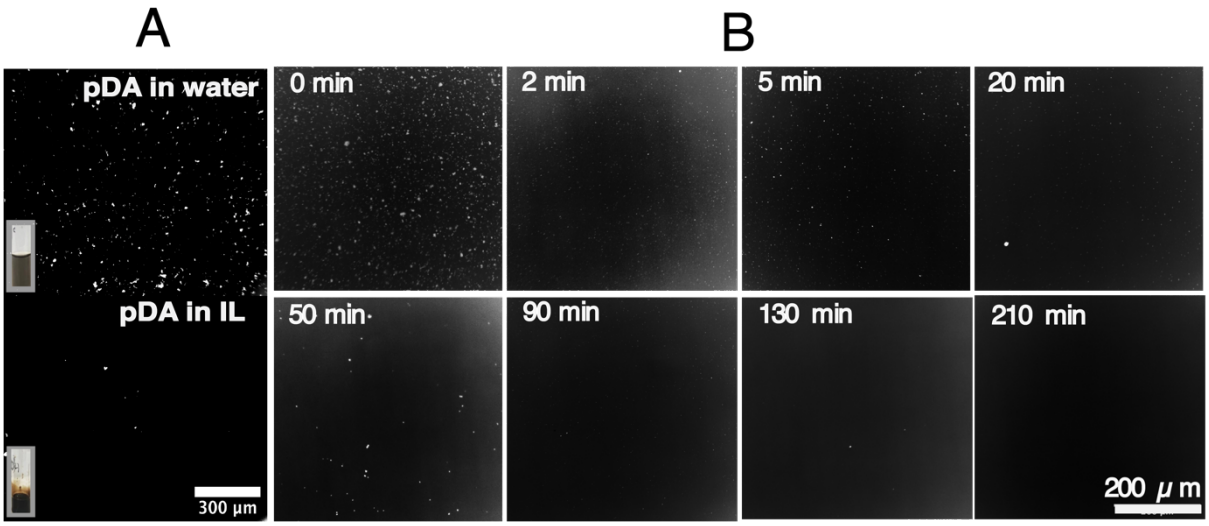

Supplementary Figure 4. Polarized optical microscopy images showing particles of pDA in **(A)** 2 mg of pDA dispensed in 2mL of water and 5 mg of pDA in 200µL of [C_2mim][OAc] **(B)** 3 mg of pDA dispensed in 200 µL [C2mim] [OAc] captured at different time intervals. The scale bar of 300 µm applies to the two images in a) and the scale bar of 200 µm applies to the eight images in b).

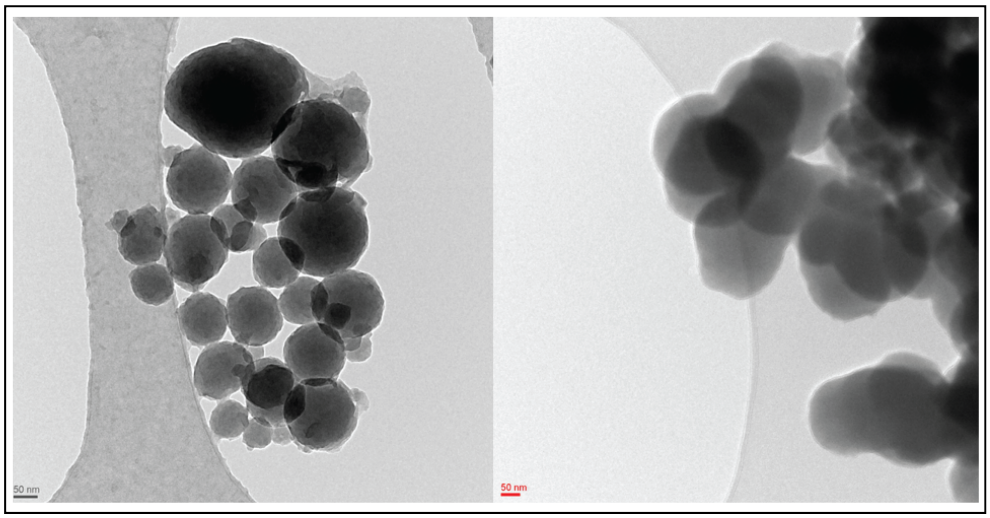

Supplementary Figure 5. Transmission electron microscopy images synthesized in TRIS and pDA recovered from IL (scale bar = 50 nm).

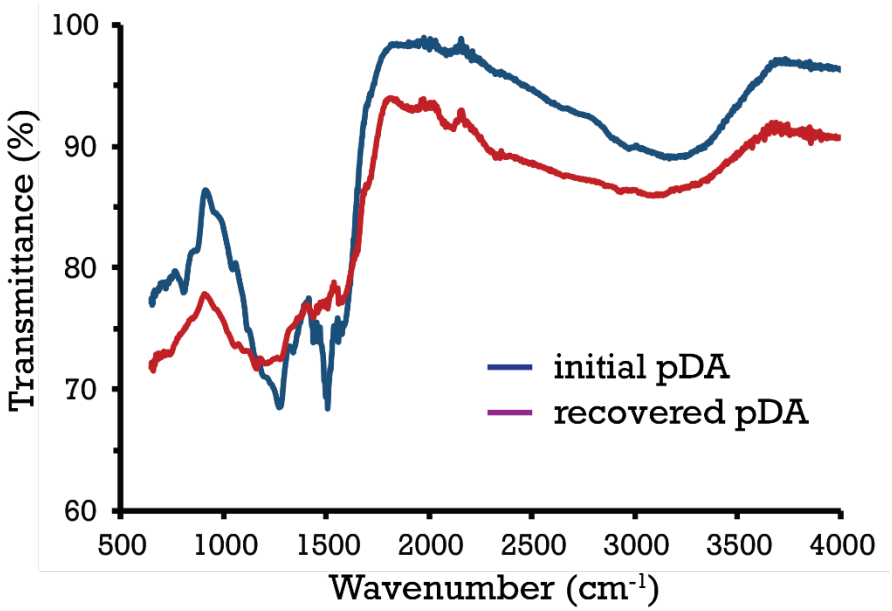

Supplementary Figure 6. Solid state FTIR of pDA synthesized in TRIS and pDA recovered from IL.

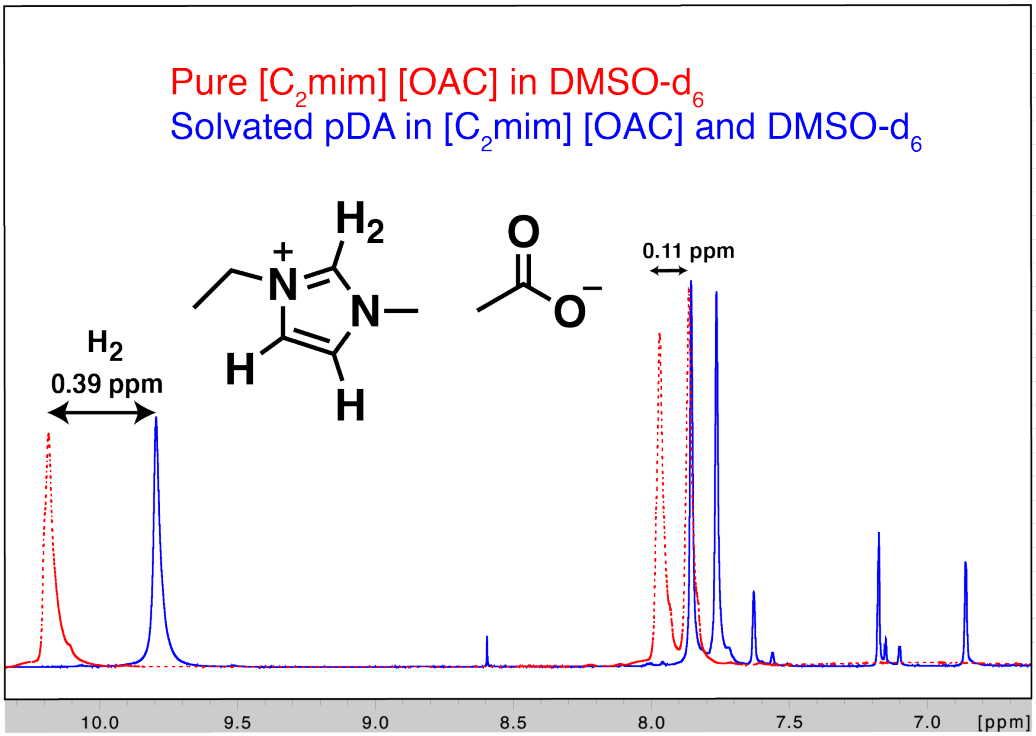

Supplementary Figure 7. ^{1}H-NMR spectra of [C2mim][OAc] (in red) and pDA - [C2mim][OAc] (blue) in DMSO-d6 .

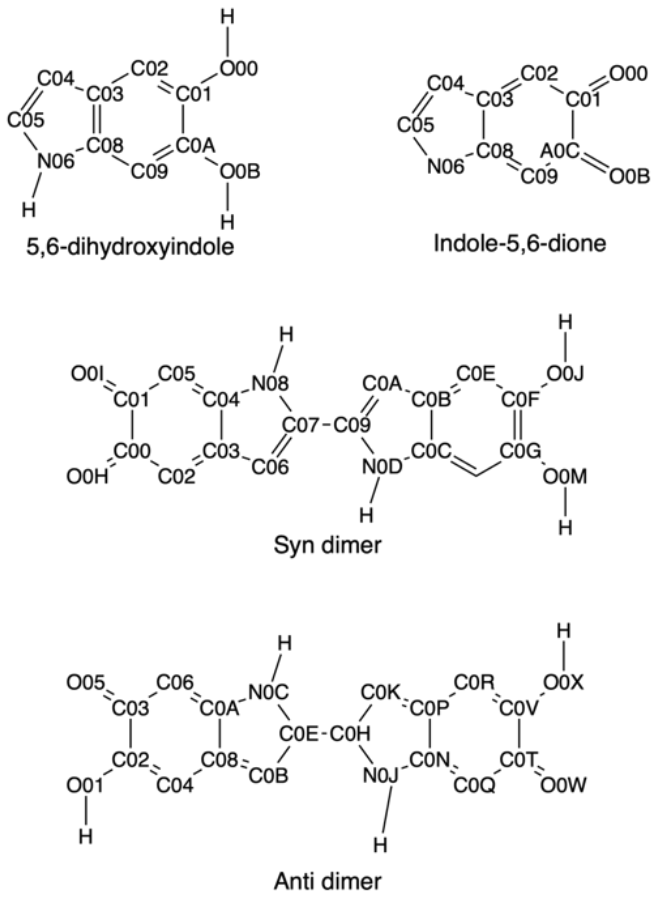

Supplementary Figure 8. Atom types of each solute used in MD simulations.

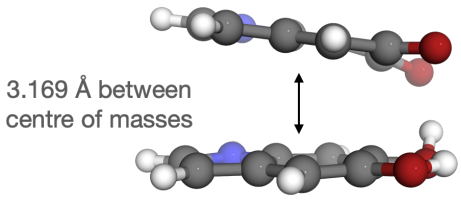

Supplementary Figure 9. Distance between the center of masses of an indoledione…dihydroxyindole π-stacked pair.

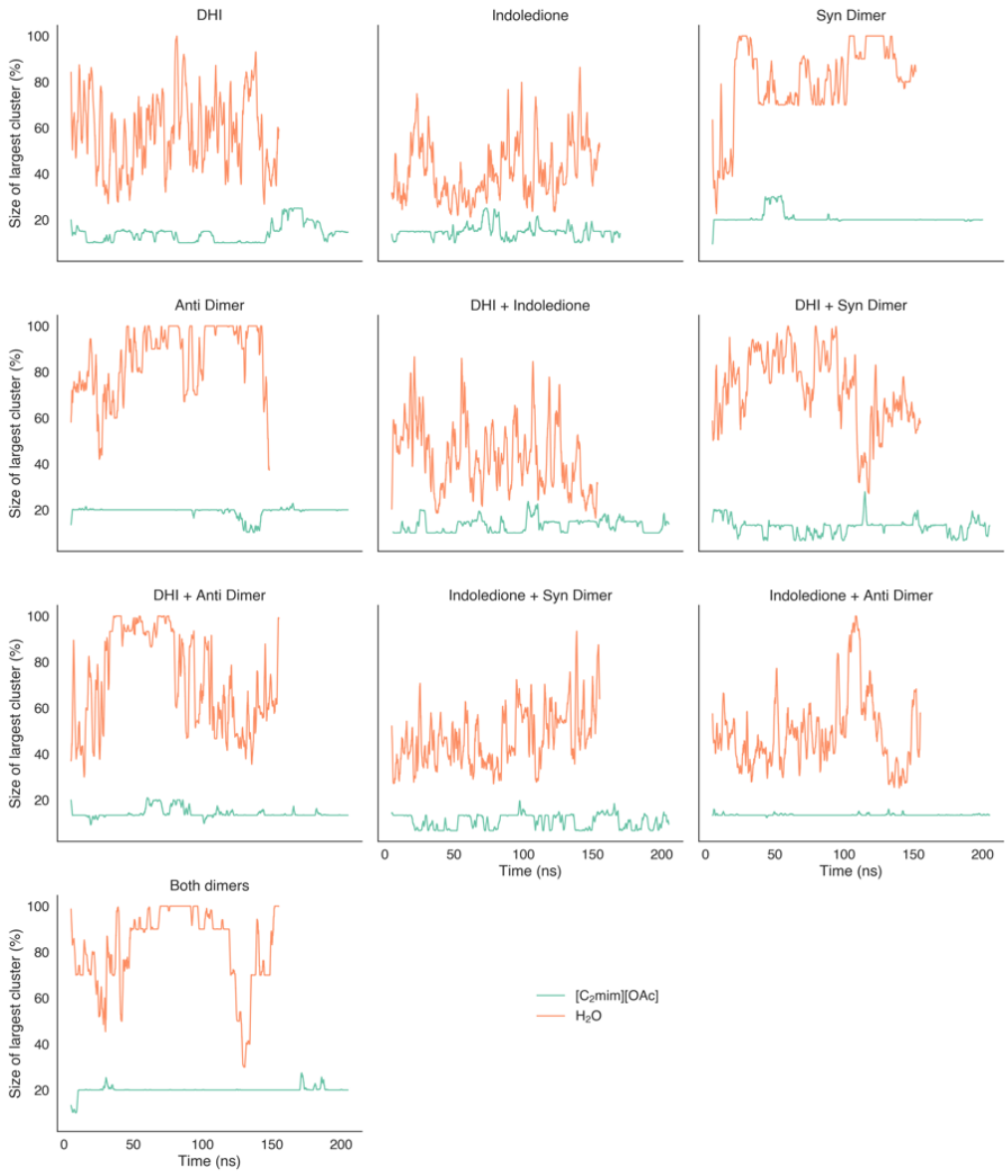

Supplementary Figure 10. Raw data produced by *gmx clustsize*, reporting the number of molecules in the largest cluster of each simulation at each timestep. Due to the varying numbers of solute molecules in each simulation, results were processed so that the size of each cluster is given as a percentage of solute molecules in each simulation. Cluster sizes were determined using a 4 Å cutoff and percentages are given to allow for comparisons between each simulation – simulations involving only monomers included 20 solute molecules, simulations involving

mixtures used 10 of each monomer and 5 of each dimer, as detailed in the theoretical section above. As an example in the case of both syn and anti dimers, there are 10 solute molecules in total, therefore when 5 molecules aggregate to form the largest cluster in that particular trajectory frame, a value of 50 % is plotted.

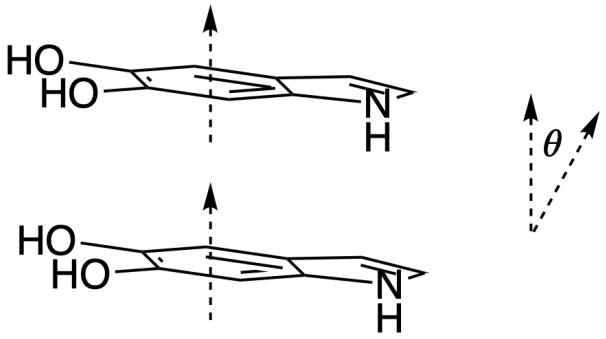

Supplementary Figure 11. Depiction of vectors used to describe the angle of π-π stacking in this study.

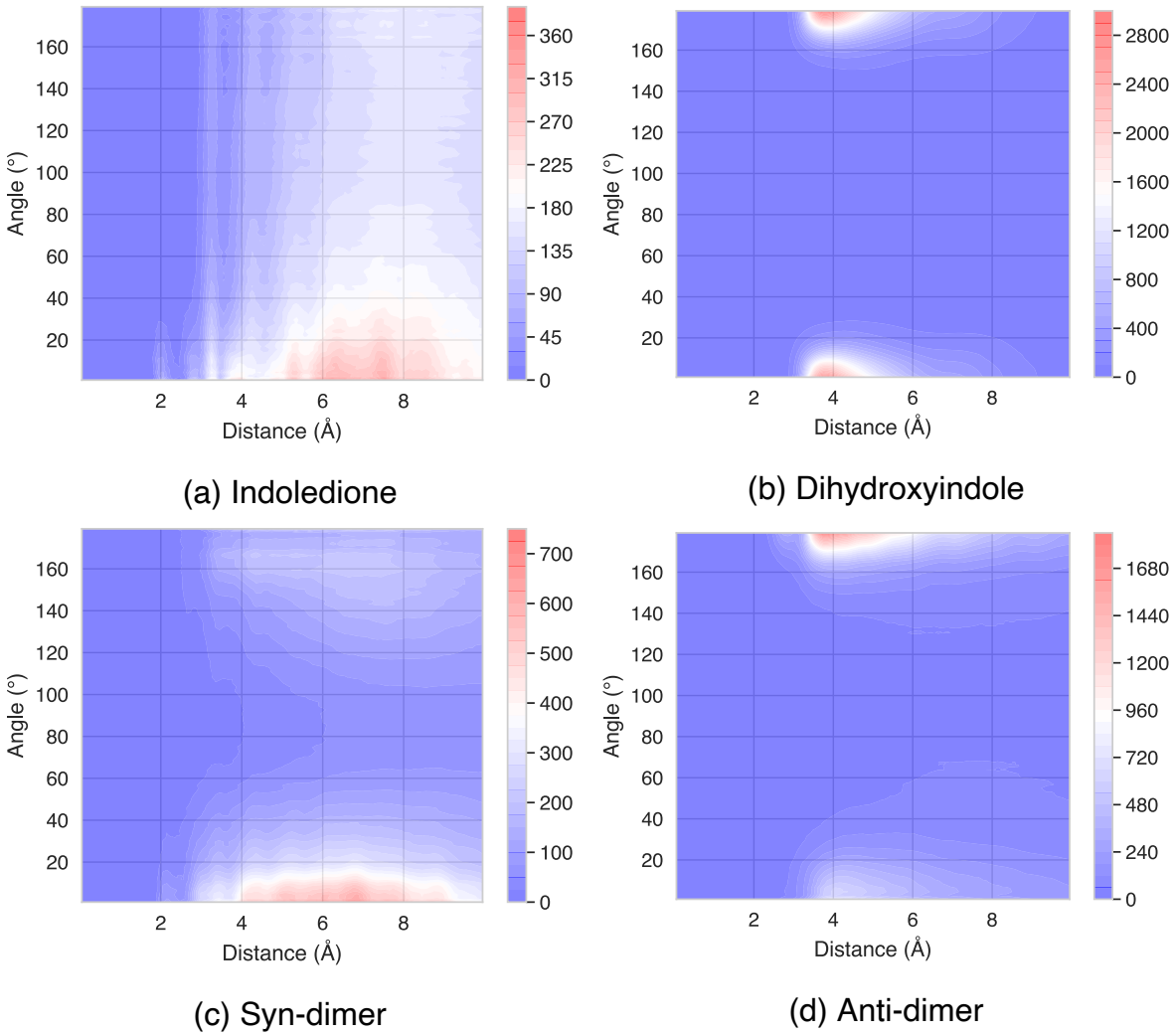

Supplementary Figure 12. Intermolecular distance-angle correlations of simulations containing one type of solute only.

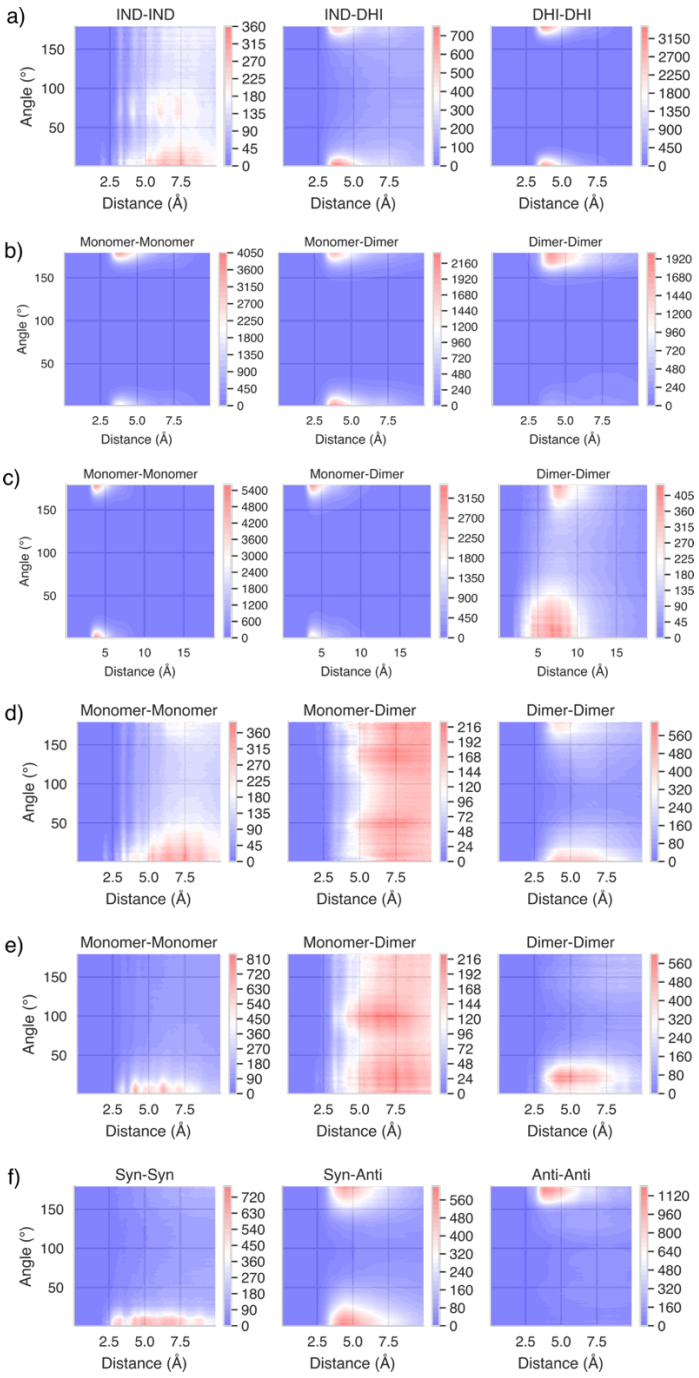

Supplementary Figure 13. Intermolecular distance-angle correlations of **a)** indoledione interacting with dihydroxyindole. **b)** dihydroxyindole interacting with the anti-dimer **c)** dihydroxyindole interacting with the syn-dimer **d)** indoledione interacting with the anti-dimer **e)** indoledione interacting with the syn-dimer **f)** syn-dimer interacting with the anti-dimer.

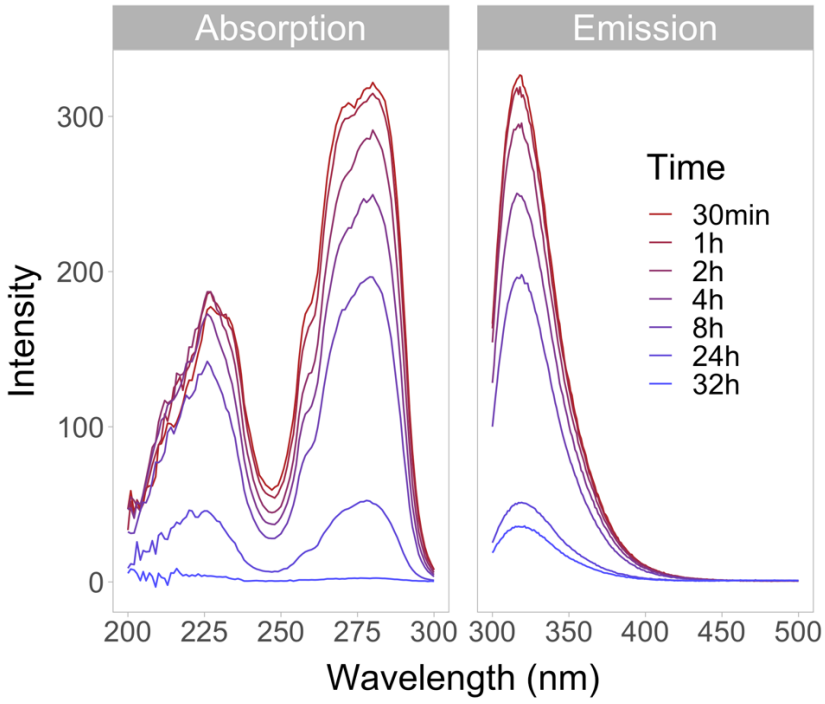

Supplementary Figure 14. Experimental absorption and fluorescence spectra of dopamine polymerized in water. Excitation and emission were studied at 280 nm and 320 nm respectively, with spectra recorded over a 32-hour period.

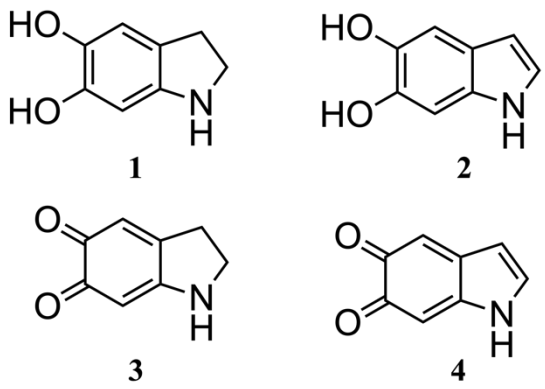

Supplementary Figure 15. Monomer variants investigated computationally.

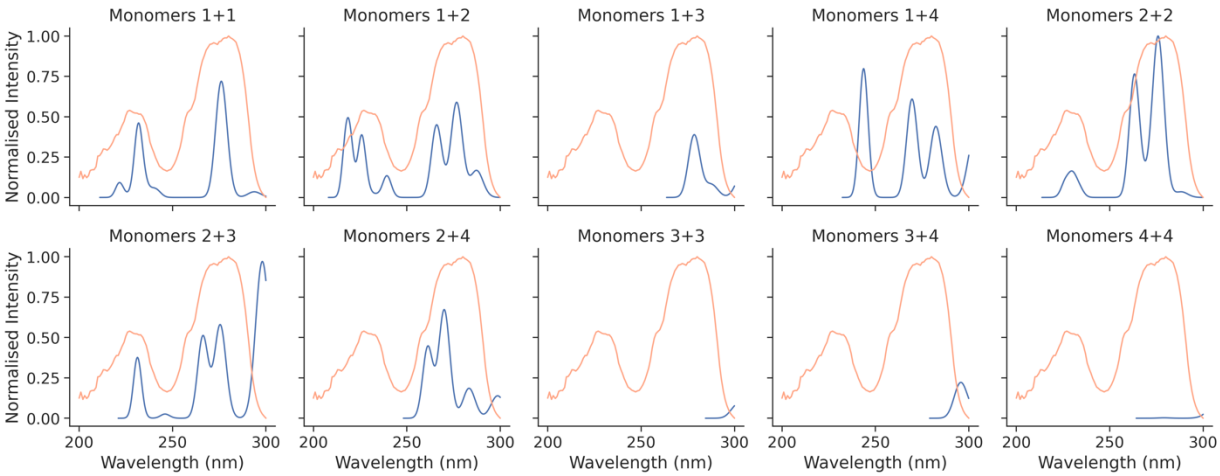

Supplementary Figure 16. Absorption of π-stacked dopamine monomers in water compared to experiment, calculated at the ωB97XD/aug-cc-pVDZ level using the SMD solvation model. Combinations of each variant in fig. S15 were used here.

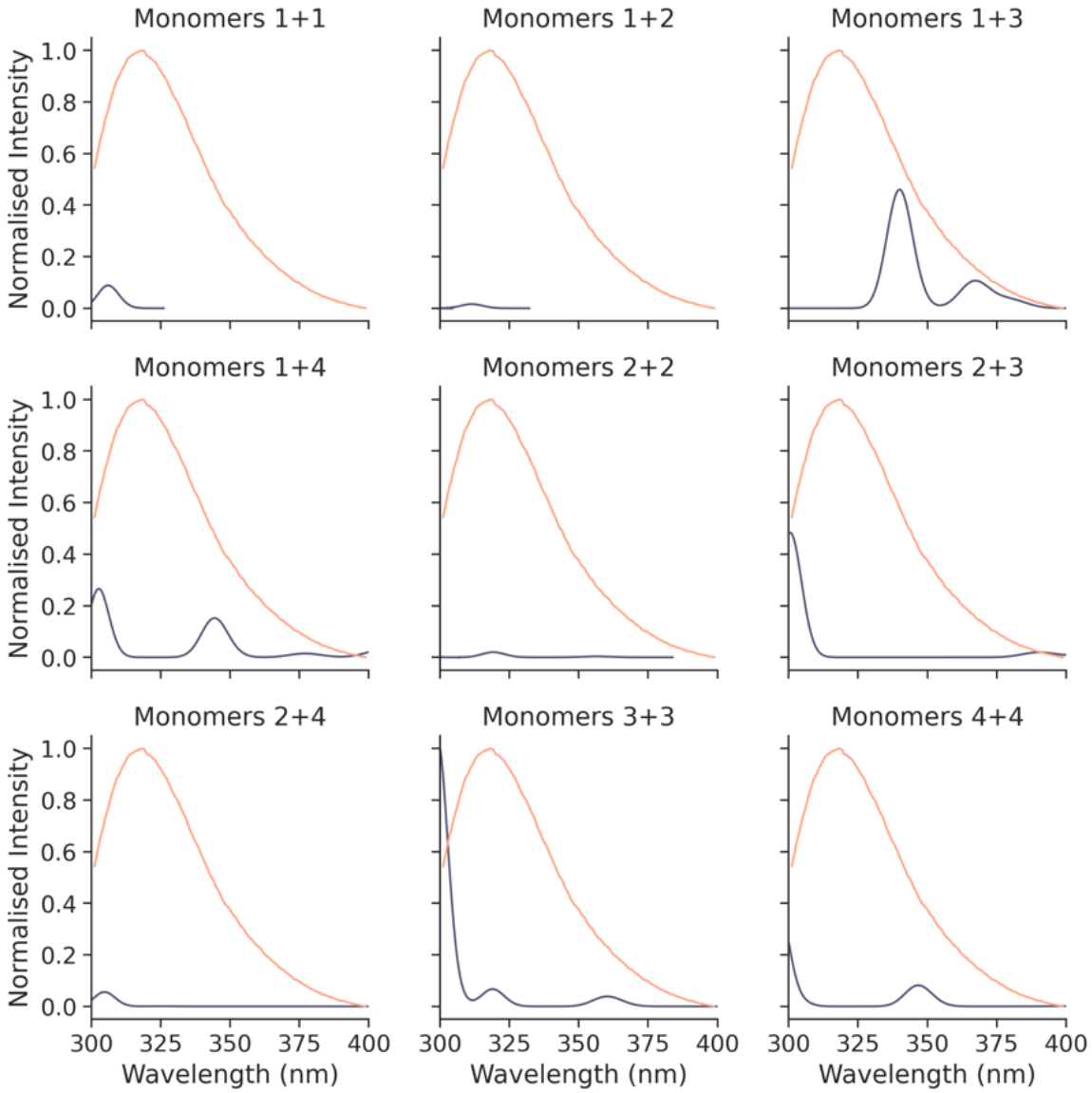

Supplementary Figure 17. Predicted fluorescence spectra of dopamine monomers outlined in fig. S14, calculated at the ωB97XD/aug-cc-pVDZ level using the SMD solvation model. Combinations of each variant in fig. S15 were used here, and the most intense emission from each combination is shown.

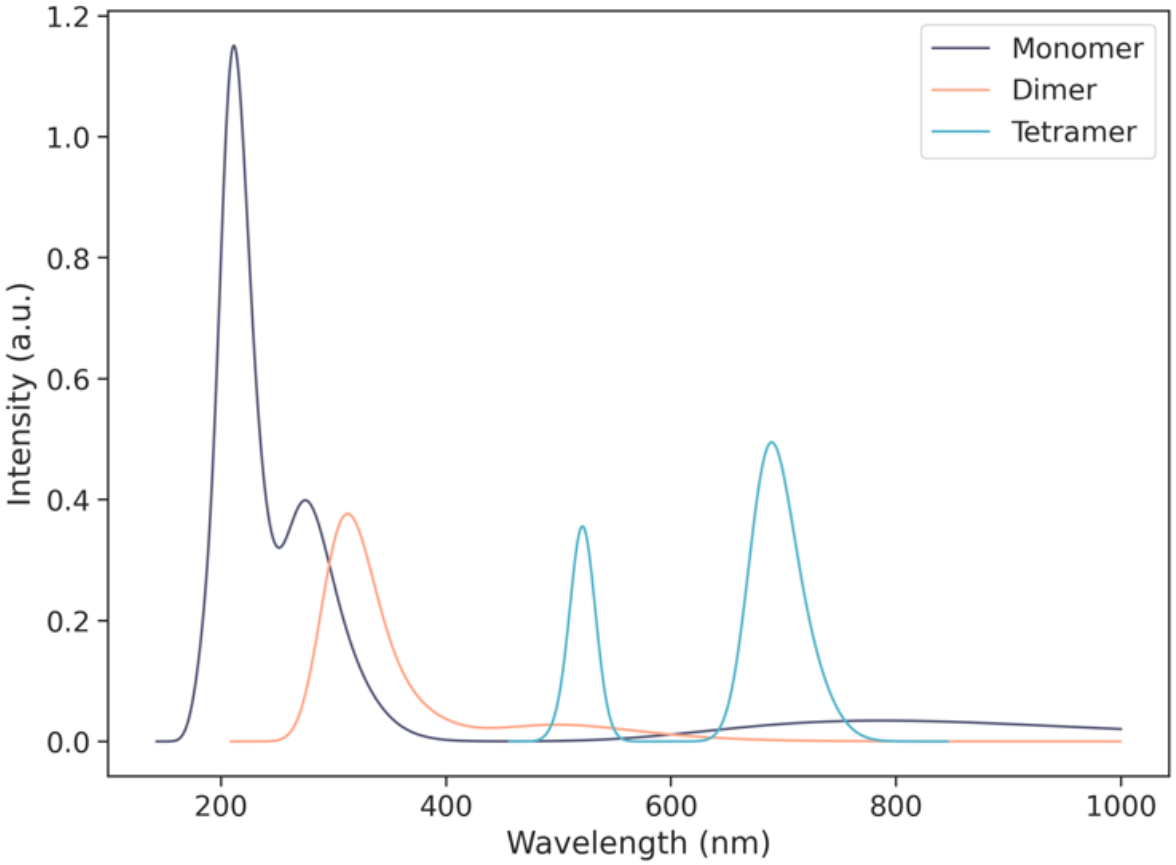

Supplementary Figure 18. Absorption of increasingly larger aggregates of monomer **4** (see Fig. 1 of the main manuscript) in fig. S12. Note the increase in wavelength as cluster size increases.

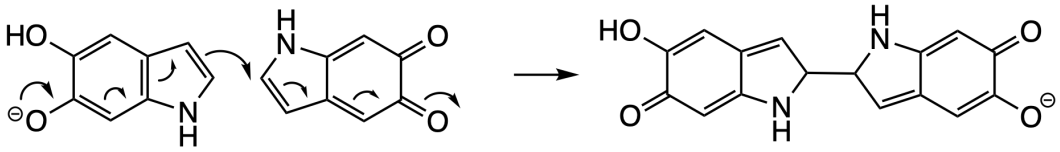

Supplementary Figure 19. Anti-dimerization of dopamine, observed in a mixture of [C_2mim][OAc] and DMSO.

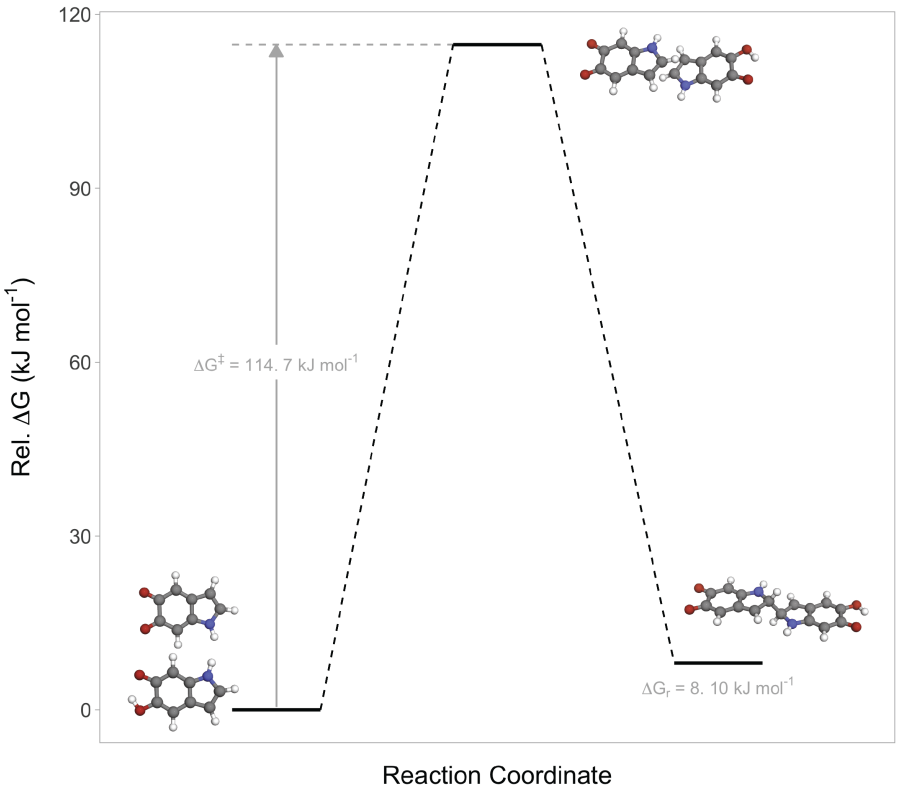

Supplementary Figure 20. Free energy barrier associated with the anti-dimerization of dihydroxyindole and indoledione found in supramolecular polydopamine.

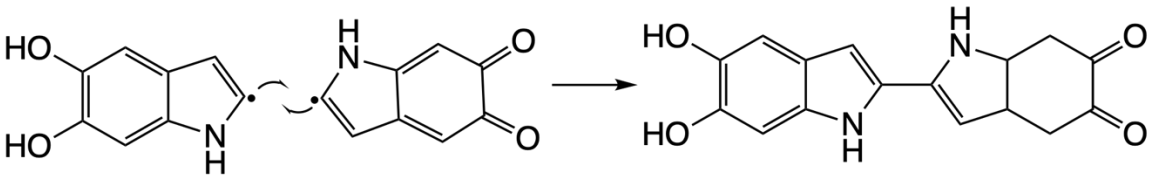

Supplementary Figure 21. Syn-dimerization of dopamine, observed in a mixture of [C_2mim][OAc] and DMSO.

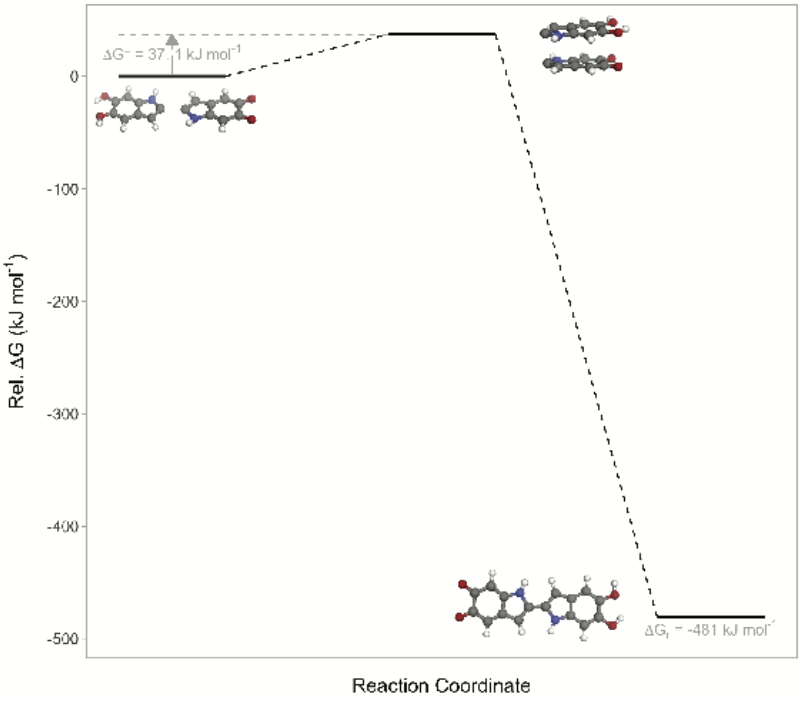

Supplementary Figure 22. Free energy barrier associated with the syn-dimerization of dihydroxyindole and indoledione found in supramolecular polydopamine.

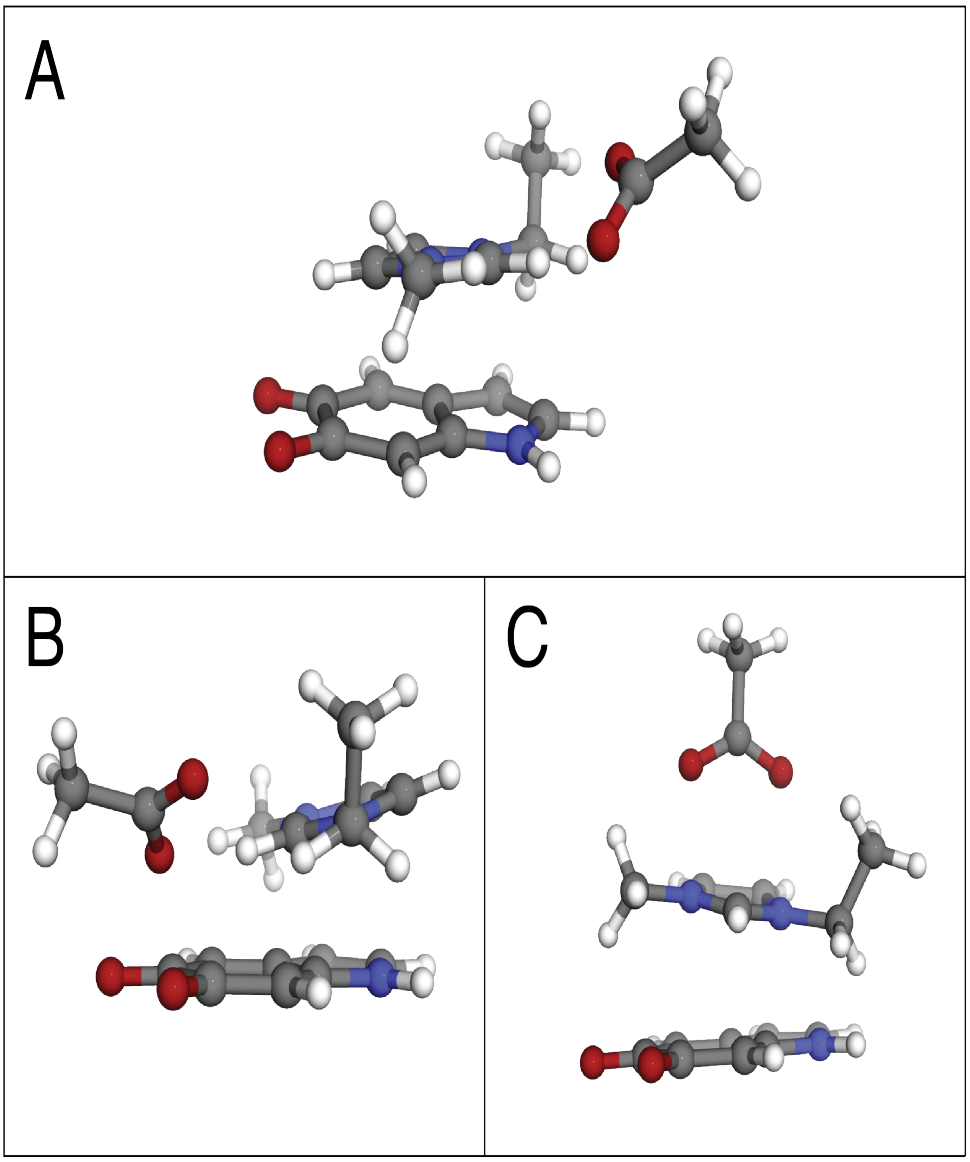

Supplementary Figure 23. Optimized configurations shown for each dopamine/IL combination: π stacking of the cation and cyclized dopamine with the carbonyls of cyclized dopamine oriented away (A) or towards (B) the anion or π stacking of the cation, anion and cyclized dopamine(C).

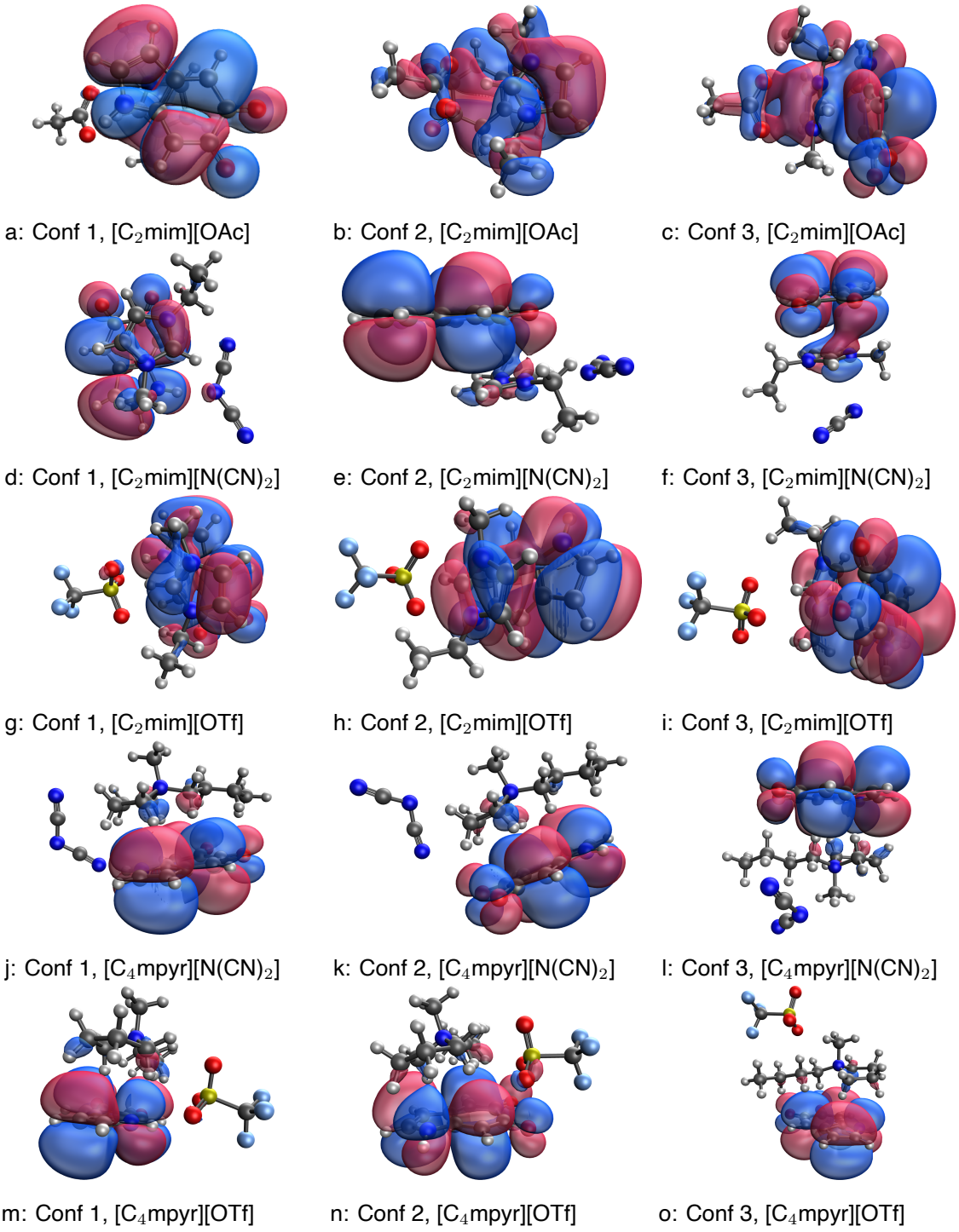

Supplementary Figure 24. HOMOs for each indoledione configuration with the five ionic liquids studied. Calculations were performed with HF/cc-pVTZ.

2. Supplementary tables

Supplementary table 1. 5,6-dihydroxyindole polarizabilities calculated at the M062X/cc-pVTZ level. Atom types correspond to those in Fig. S8. See theoretical section for more details.

Atom type	α (Å^3)
O00	0.80
C01	1.30
C02	1.36
C03	1.40
C04	1.28
C05	1.20
N06	1.10
C08	1.37
C09	1.37
C0A	1.30
O0B	0.82

Supplementary table 2. Indole-5,6-dione polarizabilities calculated at the M062X/cc-pVTZ level. Atom types correspond to those in Fig. S8. See theoretical section for more details.

Atom type	α (Å^3)
O00	1.11
C01	1.53

C02	1.55
C03	1.55
C04	1.45
C05	1.20
N06	1.18
C08	1.49
C09	1.57
C0A	1.55
O0B	1.10

Supplementary table 3. Syn dimer polarizabilities calculated at the M062X/cc-pVTZ level. Atom types correspond to those in Fig. S8. See theoretical section for more details.

Atom type	α (Å^3)
C00	1.70
C01	1.75
C02	2.00
C03	2.08
C04	2.01
C05	1.90
C06	2.04
C07	2.79
N08	1.66
C09	3.05
C0A	1.86
C0B	2.02
C0C	2.00
N0D	1.68
C0E	1.77
C0F	1.53
C0G	1.61
O0H	1.13
O0I	1.00
O0J	0.93

O0M	0.99
C0S	1.79

Supplementary table 4. Anti-dimer polarizabilities calculated at the M062X/cc-pVTZ level. Atom types correspond to those in Fig. S8. See theoretical section for more details.

Atom type	**α (Å^3)**
O01	0.90
C02	1.48
C03	1.44
C04	1.68
O05	1.13
C06	1.82
C08	1.75
C0A	1.69
C0B	1.58
N0C	1.46
C0E	1.68
C0H	1.68
N0J	1.47
C0K	1.61
C0N	1.70
C0P	1.77
C0Q	1.83

C0R	1.74
C0T	1.46
C0V	1.52
O0W	1.12
O0X	0.88

Supplementary table 5. Parameters used to determine k_{ij} values according to the regression model proposed by Padua et al.

Molecule	Charge	Dipole moment (D)	Molecular polarizability (Å^3)
C_2mim	1	1.1558	12.38
OAc	-1	3.1851	5.705
Dihydroxyindole	0	3.4446	15.291
Indoledione	0	9.4527	17.02
Syn dimer	0	11.3343	41.92
Anti dimer	0	1.7854	36.5235
Water	0	2.0249	1.382

Supplementary Table 6. Parameters used to reduce the strength of non-bonding LJ terms between molecules, accounting for the explicit polarization that Drude particles provide.

Interaction	COM separation (Å)	k_{ij}
C_2mim···OAc	4.073	0.270
C_2mim···Ind	3.401	0.780
C_2mim···C_2mim	3.056	0.714
Ind···OAc	5.345	0.331
Ind···Ind	3.800	0.938
Ind···Water	5.346	0.598

Supplementary table 7. Percentage difference in the average aggregate size across the entirety of each simulation when comparing water and [C_2mim][OAc] solvents, relative to the average

size in [C_2mim][OAc]. The calculation is explained in detail on page 4, using the output of the `gmx clustsize` program to determine aggregate sizes.

Solute	**% increase in aggregate size**
Anti Dimer	66.7
Both Dimers	62.1
DHI + Syn Dimer	60.3
Syn Dimer	60.0
DHI + Anti Dimer	58.3
DHI	44.3
Indoledione + Syn Dimer	36.3
Indoledione + Anti Dimer	35.8
DHI + Indoledione	30.1
Indoledione	26.7

Supplementary table 8. SRS-MP2 interaction energies in kJ mol^{-1} between stacked monomer pairs. Monomer numbers directly correspond to the structures in Fig S15.

Complexes of monomers considered*	Interaction energy (kJ mol^{-1})
1 + **1**	-72.7
1 + **2**	-71.4
1 + **3**	-76.6
1 + **4**	-80.7
2 + **2**	-57.4
2 + **3**	-83.5
2 + **4**	-86.0
3 + **3**	-34.9
3 + **4**	-36.9
4 + **4**	-48.5

*1 = Protonated form of dihydroxyindole, 2 = dihydroxyindole, 3 = protonated form of indoledione, 4 = indoledione.

Supplementary table 9. Electronic energies (E_{el}, in Hartrees) and thermodynamics properties* used to calculate the syn-dimerization reaction barrier.

Species	DHI anion	Indole-5,6-dione	TS	Product
ZPVE (kJ/mol)	320.90282	301.39571	630.7896	637.72456
TC (kJ/mol)	25.23229	35.83097	58.33232	56.23094
S_{total} (J/mol/K)	345.91119	404.58928	525.21016	511.66024
E_{el}(ωB97xD/aug-cc-pVTZ)	-513.72037	-513.00747	-1026.7445	-1026.7649
E_{el} (M05-2X/6-311+G**(gas))	-513.8007	-513.08666	-1026.904	-1026.9185
E_{el} (M05-2X/6-311+G**(solv))	-513.90484	-513.11534	-1027.0107	-1027.0491
$\Delta H^{\ddagger}$ (gas, kJ/mol)	-1348426.7	-1346563.9	-2695028.5	-2695077.4
$\Delta G^{\ddagger}$ (gas, kJ/mol)	-1348555.8	-1346714.9	-2695224.4	-2695268.3
$\Delta\Delta G$ (solv, kJ/mol)	-273.42552	-75.29103	-280.11192	-342.89206
ΔG (solv, kJ/mol)	-1348829.2	-1346790.1	-2695504.6	-2695611.2
Rel. ΔG (solv, kJ/mol)	0	0	114.786336	8.09964148

* ZPVE = Zero-point vibrational energy; TC = temperature correction (formula is shown in the theoretical section at the top of this document); S_{total} = Total entropy contribution ($S_{el} + S_{vib} + S_{rot} + S_{trans}$) ; E_{el} = electronic energy; $\Delta H^{\ddagger}$ = Change in enthalpy from the reactants to the transition state; $\Delta G^{\ddagger}$ = Change in Gibbs' free energy from the reactants to the transition state; $\Delta\Delta G$ = Gibbs' free energy correction to reflect solvation effects (calculated from the M05-2X/6-311+G** energies, $\Delta G_{solv} - \Delta G_{gas}$); ΔG = summation of all terms to give the total Gibbs' free energy for each species; Rel. ΔG = ΔG (TS) - ΔG (Reactants)

Supplementary table 10. Electronic energies (E_{el}, in Hartrees) and thermodynamics properties* used to calculate the syn-dimerization reaction barrier.

Species	Reactant 1	Reactant 2	TS	Product
ZPVE (kJ/mol)	251.23005	316.04037	597.45089	600.53568
TC (kJ/mol)	24.00334	26.45806	58.89356	54.94723
S_{total} (J/mol/K)	347.04976	357.33028	527.4241	501.93034
E_{el}(ωB97xD/aug-cc-pVTZ)	-512.30067	-513.56359	-1025.8945	-1026.0914
E_{el} (M05-2X/6-311+G**(gas))	-512.37501	-513.62567	-1026.0482	-1026.2456
E_{el} (M05-2X/6-311+G**(solv))	-512.39836	-513.65507	-1026.0965	-1026.2976
$\Delta H^{\ddagger}$ (gas, kJ/mol)	-1344770.2	-1348018.7	-2692829.5	-2693347.6
$\Delta G^{\ddagger}$ (gas, kJ/mol)	-1344899.7	-1348152.1	-2693026.4	-2693534.8
$\Delta\Delta G$ (solv, kJ/mol)	-61.302442	-77.169489	-126.74536	-136.37944
ΔG (solv, kJ/mol)	-1344961	-1348229.2	-2693153.1	-2693671.2
Rel. ΔG (solv, kJ/mol)	0	0	37.1102211	-481.01996

* ZPVE = Zero-point vibrational energy; TC = temperature correction (formula is shown in the theoretical section at the top of this document); S_{total} = Total entropy contribution ($S_{el} + S_{vib} + S_{rot} + S_{trans}$) ; E_{el} = electronic energy; $\Delta H^{\ddagger}$ = Change in enthalpy from the reactants to the transition state; $\Delta G^{\ddagger}$ = Change in Gibbs' free energy from the reactants to the transition state; $\Delta\Delta G$ = Gibbs' free energy correction to reflect solvation effects (calculated from the M05-2X/6-311+G** energies, $\Delta G_{solv} - \Delta G_{gas}$); ΔG = summation of all terms to give the total Gibbs' free energy for each species; Rel. ΔG = ΔG (TS) - ΔG (Reactants)

1. Dreyer, D. R., Miller, D. J., Freeman, B. D., Paul, D. R. & Bielawski, C. W. Elucidating the structure of poly(dopamine). *Langmuir* **28**, 6428–6435 (2012).
2. Hong, S. *et al.* Non-covalent self-assembly and covalent polymerization co-contribute to polydopamine formation. *Advanced Functional Materials* **22**, 4711–4717 (2012).
3. Liebscher, J. *et al.* Structure of polydopamine: A never-ending story? *Langmuir* **29**, 10539–10548 (2013).
4. della Vecchia, N. F. *et al.* Tris buffer modulates polydopamine growth, aggregation, and paramagnetic properties. *Langmuir* **30**, 9811–9818 (2014).
5. Chen, C. T., Martin-Martinez, F. J., Jung, G. S. & Buehler, M. J. Polydopamine and eumelanin molecular structures investigated with ab initio calculations. *Chemical Science* **8**, 1631–1641 (2017).
6. Ding, Y. *et al.* Insights into the Aggregation/Deposition and Structure of a Polydopamine Film. *Langmuir* **30**, 12258–12269 (2014).
7. Hong, S., Wang, Y., Park, S. Y. & Lee, H. Progressive fuzzy cation- assembly of biological catecholamines. *Science Advances* **4**, 1–11 (2018).
8. Alfieri, M. L. *et al.* Structural Basis of Polydopamine Film Formation: Probing 5,6-Dihydroxyindole-Based Eumelanin Type Units and the Porphyrin Issue. *ACS Applied Materials and Interfaces* **10**, 7670–7680 (2018).
9. Delparastan, P., Malollari, K. G., Lee, H. & Messersmith, P. B. Direct Evidence for the Polymeric Nature of Polydopamine. *Angewandte Chemie - International Edition* **58**, 1077–1082 (2019).